

Cutoff effects in Hartree–Fock calculations at leading order of chiral effective field theory

M. Sánchez Sánchez

CENBG, UMR 5797, Université de Bordeaux, CNRS, F-33170, Gradignan, France

Dao Duy Duc

IPHC, UMR 7178, Université de Strasbourg, CNRS, F-67000, Strasbourg, France

L. Bonneau*

LP2I Bordeaux, UMR 5797, Université de Bordeaux, CNRS, F-33170, Gradignan, France

(Dated: April 18, 2023)

We explore the effects on nuclear bulk properties of using regularization cutoffs larger than the nucleon mass within the chiral effective field theory with a power counting that ensures order-by-order renormalization in the two-nucleon system. To do so we calculate ground-state properties of the ^{16}O nucleus in the Hartree–Fock approach in a basis made up of plane waves confined in a cube. We find that regularization cutoff effects manifest themselves in two distinct ways: a strong sensitivity to the counter-terms in attractive singular partial waves (related to the sign of the corresponding low-energy constant) and to the correction for spurious deeply bound states (for high enough cutoffs). In fact the latter happens to deprive the Hartree–Fock approximation of yielding bound solutions in nuclei. We conclude that, when using a leading-order chiral potential in the Nogga–Timmermans–van Kolck’s power counting (with a regularization cutoff higher than the nucleon mass), one cannot produce a selfconsistent mean field free of spurious bound-state effects that can serve as a reference state for beyond-mean-field methods. For high regularization cutoffs which yield an attractive 3S_1 contact potential, one can at best incorporate in the mean-field solution a partial correction for spurious bound states. Then the remaining correction has to be added to the residual interaction in a treatment beyond the Hartree–Fock approximation. In fact a “full” correction in the 3D_2 channel, with energy shifts of the order of or somewhat larger than those recommended in [Phys. Rev. C **103**, 054304 (2021)], is possible.

I. INTRODUCTION

Nowadays ab initio nuclear-structure calculations employing chiral effective field theory (EFT) potentials in the Weinberg power counting [1–3] are as numerous as successful (see, e.g., the very recent works of Refs. [4–7]). In contrast very few studies have been carried out in the Nogga–Timmermans–van Kolck (NTvK) power counting [8], among which we can quote the works by Machleidt and collaborators [9] in nuclear matter using the Brueckner–Bethe–Goldstone approach, by Song and collaborators [10, 11] in $A = 3$ systems using the Faddeev approach, and by Yang and collaborators [12, 13] in light nuclei up to $A = 16$ using no-core shell-model and coupled-cluster approaches. Moreover some difficulties appear in $A > 4$ nuclei within the NTvK power counting according to the latter work.

Based on a study of phaseshift variation with the regularization cutoff Λ in various partial waves, Nogga and collaborators [8] argued that the Weinberg power counting does not yield renormalization-group invariant potentials and developed an alternate scheme in which the renormalization of the one-pion-exchange potential at leading order should be carried out nonperturbatively

in the low partial waves where the tensor part is attractive. In particular large cutoff values are considered beyond the chiral symmetry-breaking scale of the order of 1 GeV and spurious deeply bound two-nucleon states appear beyond the range of applicability of chiral EFT. The renormalized potential thus needs to be corrected before renormalization-group invariance beyond $A = 2$ systems can be studied, which has been done with success in Refs. [10, 11]. However the consideration of such large values of the momentum cutoff Λ and its interpretation in effective field theory is debated [14–19].

In this context we do not mean to dispute either point of view or line of approach to the problem of renormalization of the two-nucleon potential but rather to analyze how large regularization cutoffs can affect the outcome of nuclear-structure calculations. Because in several ab initio many-body methods the Hartree–Fock approximation serves as a reference solution or at least as an intermediate step, we explore the behavior of the Hartree–Fock solution with potentials at leading order of the NTvK power counting using a rather large regularization cutoff. In particular we try to understand the difficulties and deficiencies that can emerge from using a two-nucleon potential obeying the NTvK power counting at leading order, some of them met in the coupled-cluster calculations of Yang and collaborators [12] who showed that the Hartree–Fock ground-state solution at leading order in ^{16}O has to be deformed in order to obtain a (correlated)

* bonneau@lp2ib.in2p3.fr

ground-state energy below the 4α threshold.

This paper is organized as follows. In Sec. II we present the two-nucleon potential at leading order of chiral EFT in the Nogga–Timmermans–van Kolck power counting, including the determination of low-energy constants and the treatment of the spurious deeply bound states. Then we present in Sec. III our framework to implement this potential in the Hartree–Fock approximation through a confined plane-wave representation. The obtained results are shown in Sec. IV, followed by a discussion in Sec. V. Finally conclusions are drawn in Sec. VI.

II. LEADING-ORDER CHIRAL POTENTIAL

At least in the Weinberg’s and NTvK power countings, the leading order (LO) chiral potential is a two-nucleon operator of class I (according to Henley–Miller isospin classification). It is accounted for by the sum of the one-pion exchange potential (long-range part) and a contact potential (short-range part)

$$\hat{V}_{\text{LO}} = \hat{V}_{1\pi}^{(0)} + \hat{V}_{\text{ct}}^{(0)}, \quad (1)$$

where the superscript indicates that leading-order contributions only should enter the labeled terms. Although their expressions are well known we recall them in the appendix A for the sake of defining our notation and normalization conventions.

In this exploratory work we discard the electromagnetic interaction because its dominant contribution, the Coulomb potential, does not influence the qualitative conclusions that we reach and would significantly increase the computing time because of the exchange part of the potential when treated exactly (as opposed to the customary Slater approximation [20]). The latter contribution is attractive and partly counterbalance the repulsive direct contribution. As was shown in Ref. [21], the overall Coulomb contribution E_C to the ground-state energy calculated within the Skyrme–Hartree–Fock–BCS approach is well approximated by the liquid-drop expression $E_C = 0.73 Z^2 A^{-1/3} - 1.15 Z^2/A$. For example E_C represents of the order of 10% of the binding energy in the ^{16}O nucleus.

The renormalization of the one-pion exchange potential is performed in relevant partial waves in momentum space with a separable regularization function of the form

$$f_{\text{reg}}(k', k) = e^{-(k'^{2n} + k^{2n})(\hbar c/\Lambda)^{2n}}, \quad (2)$$

where Λ is the regularization cutoff and has the dimension of an energy. It cuts off high momenta in the counter term as well as in the one-pion exchange term of \hat{V}_{LO} . In this work we choose the frequently used value $n = 2$. The low-energy constants (LECs) appearing in the counter terms of the renormalized partial waves are fitted to scattering quantities.

To calculate phase shifts in the NN scattering we consider the K -matrix form of the Lippmann–Schwinger equation [22] in partial-wave momentum basis $|k(LS)JM\rangle$

$$K_{L'L}^{(SJ)}(k', k; q) = V_{L'L}^{(SJ)}(k', k) + \frac{2\mu}{N'_k \hbar^2} \times \sum_{L''} \mathcal{P} \int_0^\infty dk'' k''^2 \frac{V_{L'L''}^{(SJ)}(k', k'') K_{L''L}^{(SJ)}(k'', k; q)}{q^2 - k''^2}. \quad (3)$$

In this basis $\hbar c k$ is the norm of the relative linear-momentum vector between the two nucleons, L is the quantum number of the orbital relative motion, S is the total spin and J results from the coupling of relative orbital and total spin angular momenta. The isospin quantum number is deduced from the Pauli principle. Moreover, in Eq. (3), μ is the reduced mass of the two-nucleon system, $\mathcal{P} \int$ denotes a Cauchy principal-value integral and N'_k is a partial-wave normalization factor defined by

$$\langle k'(L'S')J'M' | k(LS)JM \rangle = N'_k \frac{\delta(k' - k)}{k'k} \delta_{L'L} \delta_{S'S} \times \delta_{J'J} \delta_{M'M}. \quad (4)$$

In Eq. (3) $V_{L'L}^{(SJ)}$ is the renormalized potential in the $^{2S+1}(L', L)_J$ partial wave.

In practice we solve Eq. (3) by approximating $\mathcal{P} \int_0^\infty$ with a Gauss–Legendre quadrature over the interval $[0; k_{\text{max}}]$ with $\hbar c k_{\text{max}} = \Lambda + 700$ MeV. The latter upper bound is found to be a satisfactory compromise between accuracy and computational speed. Once discretized the Lippmann–Schwinger equation becomes a linear system. For Λ values up to 1500 MeV, it is sufficient to use 70 points—the degree of the Legendre polynomial whose roots yield the momentum mesh by an affine transformation from $[-1; 1]$ to $[0; k_{\text{max}}]$.

A. Power counting

Let us now recall the essential aspects of Weinberg’s and NTvK power countings.

The former scheme relies on dimensional analysis. It predicts a short-range potential at leading order entering Eq. (1) of the form

$$\langle \mathbf{k}' | \hat{V}_{\text{ct}}^{(0)} | \mathbf{k} \rangle = C_s + C_t \hat{\boldsymbol{\sigma}}_1 \cdot \hat{\boldsymbol{\sigma}}_2, \quad (5)$$

where \mathbf{k}, \mathbf{k}' are incoming and outgoing relative momenta, C_s and C_t are constants, and $\hat{\boldsymbol{\sigma}}_1, \hat{\boldsymbol{\sigma}}_2$ are Pauli spin- $\frac{1}{2}$ operators. Moreover the one-pion exchange potential requires, at leading order, renormalization of its S -wave channels only. The above contact terms can thus serve this purpose and according to the Weinberg prescription, the renormalization of these partial waves has to be carried out nonperturbatively. Generally speaking, depending on the order retained to truncate the chiral expansion

of the inter-nucleon potential, one may have up to A -nucleon terms in the potential and the nonperturbative renormalization is carried out in few-body systems up to A nucleons. Typically at $N^3\text{LO}$ two-body and three-body terms appear in the chiral potential and the LECs are to be fitted on some two-nucleon and three-nucleon data. Then calculations of observables in a given nucleus proceed by using a many-body method to solve the eigenvalue equation for $\hat{H} = \hat{T}_{\text{intr}} + \hat{V}_{\text{LO}}$, where \hat{T}_{intr} is the kinetic energy operator in the center-of-mass frame of the nucleus. We consider here the (modest) Hartree–Fock approximation, which requires to solve a one-body eigenvalue equation iteratively. This is the first step in so-called beyond-mean-field calculations such as, for medium-mass or heavier nuclei, in the coupled-cluster method [23, 24], the selfconsistent Gorkov–Green’s functions method [25, 26], the projected generator coordinate method [27], the many-body perturbation theory [28–31] or the in-medium similarity renormalization group method [32–34].

In contrast, Nogga, Timmermans and van Kolck [8] advocate that, in addition to the two S waves in the Weinberg power counting, at least low- L , spin-triplet partial waves in which the tensor part of the one-pion exchange potential is attractive should be nonperturbatively renormalized. This is prompted by the singular nature of this potential. As this is the case in an infinite number of channels one could fear that infinitely many low-energy constants are necessary, depriving the theory of any predictive power. However, beyond some value of L , the centrifugal barrier is expected to provide enough repulsion to counterbalance the attractive tensor potential and produce spurious bound states beyond EFT momentum range of applicability. In practice counter-terms in at least 3P_0 , 3P_2 and 3D_2 partial waves should be promoted to leading order and treated non-perturbatively according to Ref. [8]. A detailed analysis of the centrifugal suppression taming the attractive, non singular one-pion-exchange potential has been performed in peripheral spin-singlet partial waves by Pavón Valderama and collaborators in Ref. [35]. This was translated into a power-counting demotion of the one-pion-exchange potential in singlet channels. However a similar study has not been carried out to date in spin-triplet partial waves where the tensor part of $\hat{V}_{1\pi}$ is attractive. The only related works that we are aware of are those by Birse [36], in the chiral limit of vanishing pion mass, and by Wu and Long [37].

In the NTVK scheme, the $\hat{V}_{1\pi}$ potential in partial waves other than 1S_0 , $({}^3S_1, {}^3D_1)$ (which corresponds to 3S_1 , 3D_1 and $\varepsilon_1 = {}^3S_1 - {}^3D_1$ and the hermitean conjugate), 3P_0 , 3P_2 and 3D_2 are subleading and should be treated perturbatively because for large enough cutoff Λ , the iteration of the one-pion exchange potential can become large and introduce cutoff dependence beyond the error of truncation at leading order. However for Λ below 2000 MeV or so this should not happen according to Ref. [8]. This is the approach followed in the recent no-core shell-model

calculations of Ref. [38]. Instead we adopt here a more “conservative” strategy by setting to 0 the LO potential in all partial waves other than those listed above. We call minimal scheme this approach and denote it by NTvK_{min} .

Moreover to improve the leading-order description of the 1S_0 phase shift in np scattering, we follow the work of Ref. [39] by taking into account the low-momentum scale corresponding to the zero amplitude through a dibaryon auxiliary field in the effective Lagrangian. However this produces an energy-dependent potential, easy to manipulate in a two-nucleon system but much less so in a many-nucleon system. This is why an on-shell equivalent momentum-dependent potential has been developed in Ref. [38] and abbreviated DBZ in Ref. [12]

$$V_{\text{ct}}^{({}^1S_0)}(k', k) = 4\pi \frac{(\hbar c)^3}{m_N c^2} \left[\frac{1}{\Delta_1} \mathcal{F}\left(\frac{\hbar c k'}{\gamma}\right) \mathcal{F}\left(\frac{\hbar c k}{\gamma}\right) + \frac{1}{\Delta_2} \right], \quad (6)$$

where the function \mathcal{F} is defined by $\mathcal{F}(x) = (1 + x^2)^{-1/2}$ and m_N is the nucleon mass.

In appendix B we give the results of the fitting of low-energy constants in the 1S_0 , 3S_1 , 3P_0 , 3P_2 and 3D_2 channels.

B. Treatment of spurious deeply bound states

In this work we consider three values of Λ , namely 500, 1000 and 1500 MeV. Whereas no spurious bound state is found for $\Lambda = 500$ MeV, one is supported in the 3P_0 channel for $\Lambda = 1000$ MeV, and two appear for $\Lambda = 1500$ MeV in the coupled $({}^3S_1, {}^3D_1)$ and the uncoupled 3P_0 channels. Their energies are reported in table I.

TABLE I. Spurious bound-state (negative) energies in the coupled $({}^3S_1, {}^3D_1)$ channel and the uncoupled 3P_0 , 3D_2 channels as a function of the regularization cutoff Λ . No bound state is obtained in the other channels for the considered cutoff values.

Λ (MeV)	Bound-state energies (MeV)		
	$({}^3S_1, {}^3D_1)$	3P_0	3D_2
500	–	–	–
1000	–	–418.15	–
1500	–2066.48	–234.83	–1352.39

We obtain these bound states using the Lagrange-mesh method [40] in momentum space in each partial-wave channel with the Lagrange–Legendre mesh over the interval $[0; k_{\text{max}}]$ where $\hbar c k_{\text{max}} = \Lambda + 700$ MeV as for solving the Lippmann–Schwinger equation. For Λ values up to 1500 MeV, a 70-point Lagrange–Legendre mesh has been checked to be largely sufficient. The wave function in momentum space $\chi_i^{(X)}(k)$ of the bound state $|\chi_i\rangle$ in

the channel X is real and normalized to unity as

$$\frac{1}{N'_k} \sum_{L \in X} \int_0^\infty dk k^2 [\chi_{i,L}^{(X)}(k)]^2 = 1, \quad (7)$$

where the sum over relative orbital momentum L is restricted to the values relevant to the channel X . In our implementation the bound-state wave functions are tabulated at mesh points and interpolated using the cubic Hermitean spline method Ref. [41] frequently used in few-body calculations. In addition, for low momenta between 0 and the lowest one of the mesh, we use a parabolic extrapolation from the first three tabulated values (at the lowest-three mesh points). The resulting wavefunctions in momentum space are plotted in figure 1 for the regularization cutoff $\Lambda = 1500$ MeV. Only one spurious

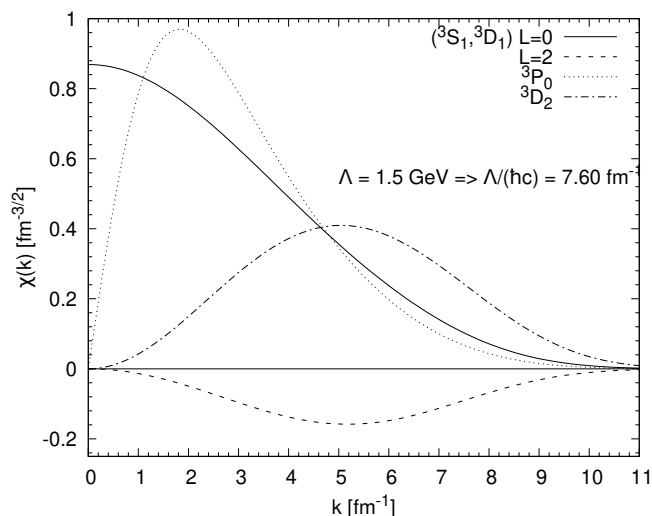


FIG. 1. Momentum-space wavefunctions of the spurious deeply bound state in the $({}^3S_1, {}^3D_1)$, 3P_0 and 3D_2 channels for $\Lambda = 1500$ MeV as functions of k .

bound state is supported in the considered partial waves, so their wave function have no node. For larger values of Λ , additional deep bound states appear [10] and one can expect that their wave functions have an increasing number of nodes.

Once the bound-state wavefunctions are known, the removal of the spurious bound states $|\chi_i\rangle$ from the two-nucleon potential \hat{V} can be done by adding a scaled projector on these bound states as in Ref. [8]. The corrected potential \hat{V}' thus reads

$$\hat{V}' = \hat{V} + \sum_i E_{\text{shift}}^{(i)} |\chi_i\rangle\langle\chi_i| \quad (8)$$

where the energy shifts $E_{\text{shift}}^{(i)}$ are large, positive constants in relevant partial-wave channels generically numbered i . According to Yang and collaborators [12], sufficiently large values are of the order of 10 to 15 GeV. We have

checked that for any value of $E_{\text{shift}}^{(i)}$ the scattering properties calculated by solving the Lippmann–Schwinger equation using the above numerical method with the potential \hat{V}' (in partial waves supporting spurious bound states) are unchanged. This is true for any cutoff value Λ . Because we work in the momentum partial-wave basis, this treatment of spurious bound states and the scattering benchmark is straightforward and efficient. The Lagrange-mesh method in partial-wave representation is thus a powerful alternative to the harmonic-oscillator basis as implemented in the NCSM calculations of Ref. [12]. It is worth mentioning that Wendt and collaborators developed an alternative method to decouple spurious deeply bound states in the SRG framework [42], which allows for a softening of the two-nucleon potential for many-body calculations at the same time but at the price of inducing three-body forces and higher.

In figures 2 and 3 we show momentum-space diagonal matrix elements of the corrected potential \hat{V}' in the $({}^3S_1, {}^3D_1)$, 3P_0 and 3D_2 channels for $\Lambda = 1500$ MeV and an energy shift $E_{\text{shift}}^{(i)} = 1$ GeV as an example. Because the $L = 0$ and $L = 2$ components of the spurious bound-state wavefunction in the deuteron channel have constant and opposite signs as functions of k , the projector contributions to the diagonal channels 3S_1 and 3D_1 are repulsive whereas it is attractive in the coupled partial-wave channel ε_1 . Similarly the momentum wavefunction of the 3P_0 bound state having zero node, it is of constant sign and the corresponding contribution to the corrected potential is repulsive. From these plots it is clear that the larger is the energy shift, the more repulsive is the corrected potential in diagonal channels, the relevant ones at leading order for Λ up to 1500 MeV being 3S_1 and 3P_0 . However it is remarkable that, for $\Lambda = 1500$ MeV, the corrected 3P_0 -projected potential is virtually equal to the energy-shifted projector as the contribution from the counter-term virtually vanishes. This is a highly non trivial effect of the nonperturbative renormalization in the 3P_0 channel.

For comparison purposes and later discussion, we also display in figure 3 the diagonal matrix elements of \hat{V}_{LO} in the 1S_0 and 3P_2 channels as functions of relative momentum. It is worth noting the repulsive contribution at moderate and high momenta (for k above 1 fm^{-1}) introduced in the 1S_0 channel by the di-baryon formalism and the fit of its LECs to the amplitude zero.

III. HARTREE–FOCK APPROXIMATION IN A CONFINED PLANE-WAVE BASIS

To implement the Hartree–Fock approximation to nuclear bound states, we represent the single-particle states in a basis made of plane waves confined in a cube, of edge length L , centered at the center-of-mass of the nucleus, to which we add the nucleon spin projection $\sigma = \pm\frac{1}{2}$ on a chosen axis (here the z axis) and the isospin projection $\tau = \pm\frac{1}{2}$. This representation was first considered by van

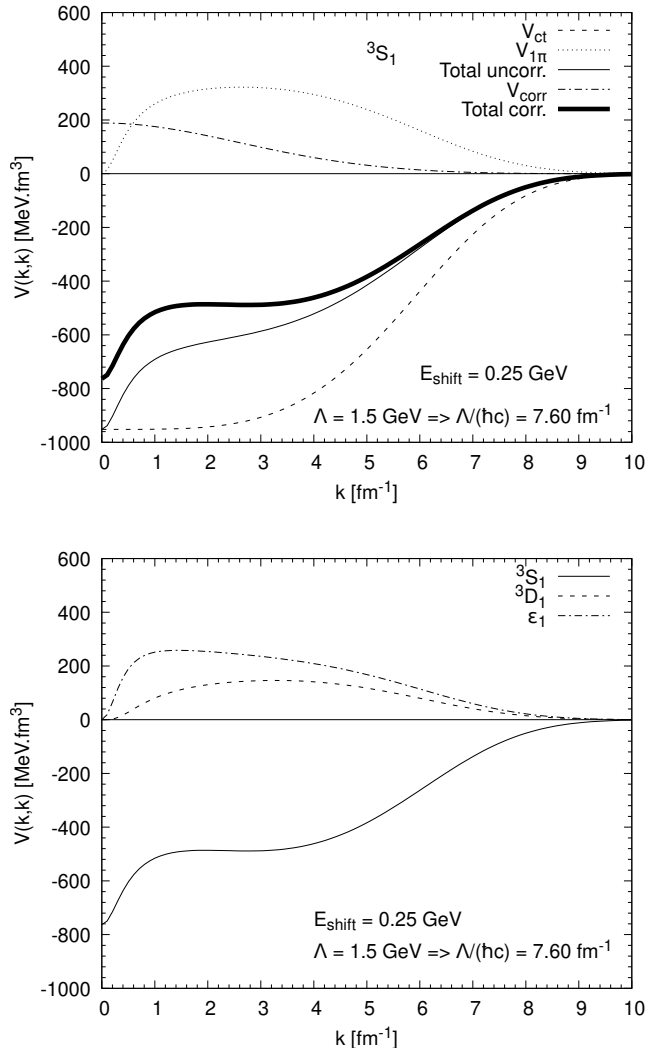


FIG. 2. Top panel: Diagonal matrix elements of the corrected potential in the 3S_1 channel as functions of relative momentum k for $\Lambda = 1500$ MeV. The contact V_{ct} and one-pion-exchange $V_{1\pi}$ contributions are plotted with regularization, as dashed and dotted lines respectively. The energy-shift applied to the spurious bound states is 1 GeV as an example. Lower panel: Diagonal matrix elements of the potential corrected for spurious bound states in the 3D_1 and ϵ_1 channels, compared with those in the 3S_1 channel, as functions of k .

Dalen and Mütter [43] (at least in Nuclear Physics) and more recently studied in details in Refs. [44, 45]. Here we summarize in this section its essential aspects.

The implementation of the confined plane-wave basis to represent the two-body matrix elements of the most general class-I, II and III potential and to solve the Hartree–Fock equations resulted in the so-called **HFchiral** code. All numerical details and algorithms can be found in Ref. [44]. We may put forward three main advantages of this code:

(i) it allows to easily describe non spherical shapes,

especially triaxial ones;

(ii) as shown in Appendix C, when the cubic box is large enough, the two-body matrix elements of the potential are proportional to those in between relative momenta. No recourse to any transformation from the center-of-mass frame to the laboratory frame is thus necessary;

(iii) there is a direct relation between the cutoffs on single-particle and relative momenta. Indeed, following van Dalen and Mütter [43], the single-particle basis size, for a fixed edge length L , is controlled by a truncation on the norm of the momentum vector. This truncation scheme is rotationally invariant and thus preserves the octahedral symmetry of the basis. The corresponding single-particle momentum cutoff is denoted by k_{\max} and, if the potential matrix elements $\langle \mathbf{k}_{\alpha'} | \hat{V} | \mathbf{k}_{\alpha} \rangle$ had a sharp cutoff $\Lambda/(\hbar c)$ on the norm of relative momenta \mathbf{k}_{α} and $\mathbf{k}_{\alpha'}$, we would then also have a sharp cutoff $k_{\max} = \Lambda/(\hbar c)$ on single-particle momenta.

Of course a more efficient implementation of the Hartree–Fock equations is possible when restricting calculations to spherically symmetric solutions, as in the ground state of ${}^{16}\text{O}$. However, the **HFchiral** code is meant to be used in deformed nuclei.

In the present work we restrict the nuclear shapes to triaxial ones by building a basis of reducible co-representation of the full octahedral double group with time-reversal symmetry \hat{T} , denoted by O_{2h}^{DT} . This symmetry-adapted basis allows to describe time-reversal symmetry breaking by the mean field, as in odd-mass nuclei. However, because the confined plane-wave basis (see Appendix C for its construction and interpretation) is invariant by \hat{T} , it is also possible to describe time-reversal invariant solutions exactly (\hat{T} is then a so-called selfconsistent symmetry).

The full symmetry group of plane waves confined in a cube being a subgroup of $SU(2)$, our Hartree–Fock calculations break spherical symmetry which nevertheless can be approximately recovered as the box size L increases. Moreover the $j = \frac{1}{2}$ and $j = \frac{3}{2}$ irreducible representations of $SU(2)$, of dimensions 2 and 4, respectively, are each decomposed in a single irreducible representation of O_{2h}^{DT} . This means that for nuclei up to $N = 8$ and/or $Z = 8$ the spherical symmetry breaking of the mean field can be tamed. Indeed, our Hartree–Fock ground-state solutions $|\Phi\rangle$ in ${}^{16}\text{O}$ are such that $\langle \Phi | \hat{J}_z | \Phi \rangle = 0$, where \hat{J}_z is the component along the z axis of the total angular-momentum operator $\hat{\mathbf{J}}$. However we do not expect that $\langle \Phi | \hat{\mathbf{J}}^2 | \Phi \rangle = 0$. To estimate the deviation from exact spherical symmetry, we calculate the hexadecapole moments $\langle \Phi | \hat{Q}_{4\mu} | \Phi \rangle$ and $\langle \Phi | r^4 | \Phi \rangle$. As was shown in [46, 47]

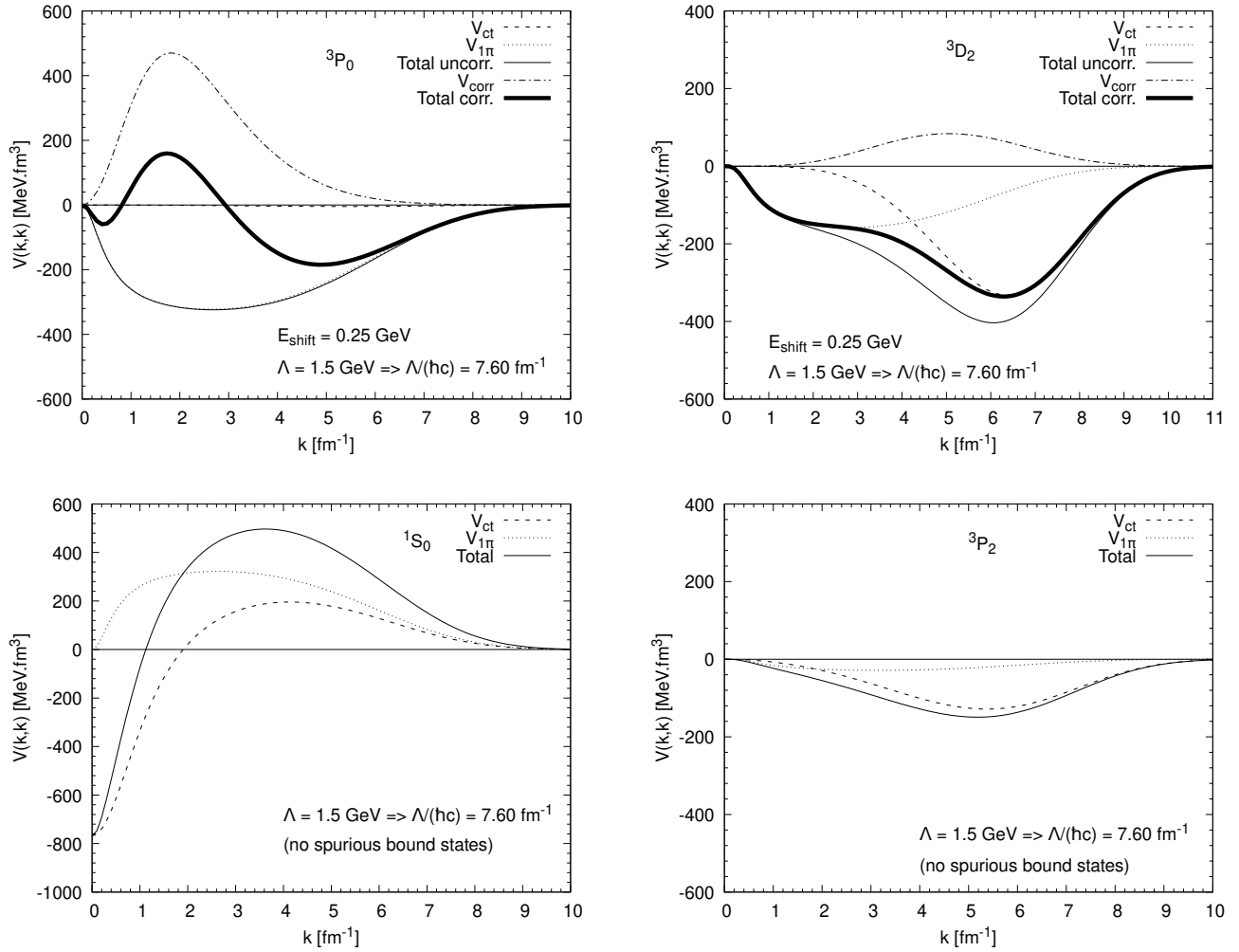


FIG. 3. Same as top panel of figure 2 in the 3P_0 and 3D_2 channels (top row) and in the 1S_0 and 3P_2 channels (bottom row). No spurious bound-state correction is necessary for the latter channels.

the relations

$$\langle \Phi | \hat{Q}_{\lambda\mu} | \Phi \rangle = 0 \quad \forall \mu \in \{-\lambda, \dots, \lambda\} \text{ and } \lambda = 2, 3 \quad (9a)$$

$$\langle \Phi | \hat{Q}_{44} | \Phi \rangle = \langle \Phi | \hat{Q}_{4-4} | \Phi \rangle = -\sqrt{\frac{5}{14}} \langle \Phi | \hat{Q}_{40} | \Phi \rangle \quad (9b)$$

$$\langle \Phi | \hat{Q}_{4\mu} | \Phi \rangle = 0 \quad \forall \mu \in \{\pm 1, \pm 2, \pm 3\} \quad (9c)$$

are characteristic of a solution $|\Phi\rangle$ with purely octahedral symmetry, as far as hexadecapole moments are concerned (similar relations hold for higher multipoles). Therefore the deviation from the spherical shape in such a solution is essentially encoded in the Bohr axial-hexadecapole deformation parameter β_4 , which can be approximated to first order as

$$\beta_4 \approx \frac{4\pi}{7} \frac{\langle \Phi | \hat{Q}_{40} | \Phi \rangle}{\langle \Phi | r^4 | \Phi \rangle}. \quad (10)$$

In this context, provided the box size parameter L is large enough, we expect a weak lowering of the ground-state

energy if angular-momentum projection is performed after the Hartree–Fock calculation. This corresponds to calculations where a small deviation $|\beta_4|$ from spherical shapes occurs, typically less than about 0.01.

In a finite discrete orthonormal basis, the Hartree–Fock equations, resulting from the variational principle applied to a Slater determinant trial wave function [48], takes the usual form of an eigenvalue equation for the single-particle Hartree–Fock Hamiltonian \hat{h}_{HF} . This one-body operator is defined by its matrix elements between any single-particle states $|a\rangle$ and $|b\rangle$ (containing all quantum numbers)

$$\langle a | \hat{h}_{\text{HF}} | b \rangle = \left(1 - \frac{1}{A}\right) \langle a | \frac{\hat{\mathbf{p}}^2}{2m_N} | b \rangle + \sum_{i \in \Phi} \langle ai | \hat{V} + \hat{T}_2 | \tilde{b}i \rangle \quad (11)$$

where i labels all single-particle states occupied in the Slater determinant $|\Phi\rangle$, \hat{T}_2 is the two-body correction to

the kinetic energy

$$\hat{T}_2 = - \sum_{1 \leq \mu < \nu \leq A} \frac{\hat{\mathbf{p}}_\mu \cdot \hat{\mathbf{p}}_\nu}{m_N}$$

and $|\tilde{b}i\rangle = |bi\rangle - |ib\rangle$ accounts for direct and exchange contributions, respectively, to the two-body matrix element. The factor $1/A$ results from the one-body kinetic-energy correction because at leading order neutrons and protons have the same mass. The kinetic-energy operator \hat{T}_{intr} in the center-of-mass frame (also called intrinsic kinetic energy) thus reads

$$\hat{T}_{\text{intr}} = \left(1 - \frac{1}{A}\right) \sum_{\mu=1}^A \frac{\hat{\mathbf{p}}_\mu^2}{2m_N} - \sum_{1 \leq \mu < \nu \leq A} \frac{\hat{\mathbf{p}}_\mu \cdot \hat{\mathbf{p}}_\nu}{m_N}. \quad (12)$$

Since the occupied states $|i\rangle$ are eigenstates of \hat{h}_{HF}

$$\hat{h}_{\text{HF}}|i\rangle = e_i |i\rangle \quad (13)$$

where e_i denotes the single-particle energy, the eigenvalue equation Eq. (13) is solved iteratively, from an initial one-body potential chosen to be a Woods–Saxon potential with central and spin orbit contributions. Owing to symmetries imposed to \hat{h}_{HF} , parity p , z -signature r_z and isospin projection τ are good quantum numbers in the present work, so the Hartree–Fock equations (13) are solved independently for each of the four combinations of (p, r_z) for neutrons and protons separately. In nuclei with $N \neq Z$ the single-particle Hartree–Fock Hamiltonian is different for neutrons and protons even if the potential \hat{V} is of class I (which is the case here at leading order for the strong interaction and in the absence of the electromagnetic interaction).

IV. RESULTS

We use the `HFchiral` code developed by two of the authors (see Refs. [44, 45]) along the lines of section III to calculate ground-state bulk properties of the ^{16}O nucleus with the leading-order two-nucleon potential described in section II.

As explained in the previous section two parameters characterize our truncated single-particle basis, namely the edge length L of the confining cubic box and the single-particle momentum cutoff k_{max} . The former establishes a natural infra-red (IR) momentum scale $\lambda_{\text{IR}} = \frac{\pi}{L}$, whereas the latter directly defines an ultra-violet (UV) relative-momentum cutoff $\lambda_{\text{UV}} = k_{\text{max}}$. In order to obtain UV convergence one should choose λ_{UV} somewhat larger than the regularization cutoff Λ of the NN potential, whereas large L values guarantee IR convergence. Contrary to the spherical harmonic-oscillator (SHO) basis, the IR and UV momentum scales are independent of each other in the confined plane-wave basis.

To get an estimate of a “reasonable” value for L and to reach a compromise between accuracy and computation

resources, we assume the nuclear mean-field potential to have the form of a Woods–Saxon potential

$$V_{\text{WS}}(r) = - \frac{V_0}{1 + e^{(r-R)/a}} \quad (14)$$

where $R = R_0 A^{1/3}$ is the empirical nuclear radius, with $R_0 \approx 1.35$ fm, V_0 is the depth of the potential and a the diffuseness parameter. The box size L should be large enough to cover the range of an eigenfunction of the corresponding hamiltonian, namely

$$L = 2R + \eta_a \times 2a + \eta_E \times \lambda_E. \quad (15)$$

In this expression $\lambda_E = \frac{\hbar c}{\sqrt{-2mc^2 E}}$ is the binding wave length (inverse of the binding momentum) and E is the energy of the last occupied nucleon (Fermi level) in the Woods–Saxon Hamiltonian neglecting spin-orbit. In the form (15) of L , the first two contributions give the radius R_{WS} at which the Woods–Saxon potential can be considered to vanish. Then for $r > R_{\text{WS}}$ the wavefunction of the bound state exponentially decays according to its eigenenergy $E < 0$, with a characteristic length λ_E . The third contribution to L in Eq. (15) thus corresponds to the distance beyond R_{WS} at which the bound-state wave function can be considered to vanish. The numerical parameters η_a and η_E are of the order of a few units so that the single-particle wave function can be considered to be approximately zero on the edge of the box. Taking $V_0 = 70$ MeV and $a = 0.7$ fm as typical values, we find a Fermi energy $E = -32.7$ MeV. We have checked that choosing $\eta_a = \eta_E = 3$ is enough to converge all bound states in this potential. This results in $L = 13.4$ fm. As shown by numerical results below, IR convergence will be actually reached for slightly smaller values.

A. Results for a low regularization cutoff

We begin with the regularization cutoff $\Lambda = 500$ MeV which corresponds to a somewhat soft NN potential. This enables us to avoid the spurious-bound state problem and to thoroughly probe the IR and UV convergences with our available computing resources.

In Fig. 4 we plot the ground-state energy and the charge radius as functions of k_{max} for $L = 10.0$ fm (dashed line and open symbols) and $L = 13.4$ fm (full line and filled symbols). The dotted lines represent the converged values of E_{HF} and r_c . One clearly observe UV convergence for $k_{\text{max}} \gtrsim 3.5$ fm $^{-1}$, somewhat higher than the NN potential regularization cutoff $\Lambda/(\hbar c) \approx 2.53$ fm $^{-1}$. Moreover the converged value for each observable is the same at the scale of the figure for both box sizes, which shows IR convergence. Finally we checked that, for both box sizes $L = 10$ fm and $L = 13.4$ fm, the expectation values of the hexadecapole moments in the Hartree–Fock ground-state solutions $|\Phi\rangle$ obey the relations (9a) to (9c). Moreover we find β_4 values of are of the order of a few thousandths.

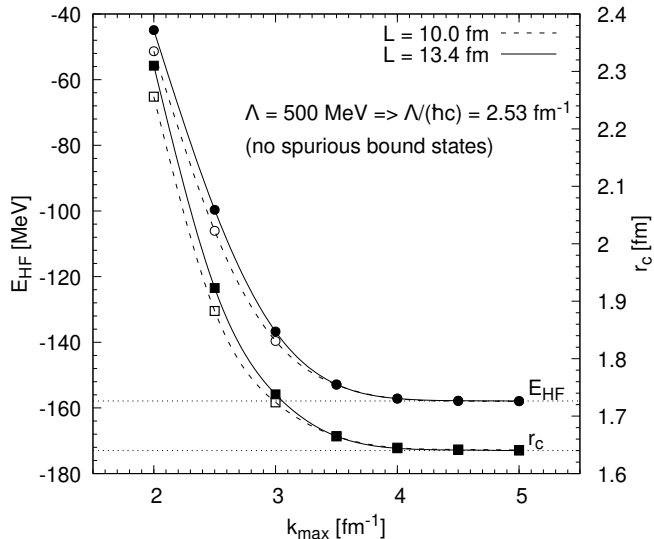


FIG. 4. Ground-state energy E_{HF} (circles, left scale) and charge radius r_c (squares, right scale) in the Hartree–Fock solution of ^{16}O as functions of the single-particle momentum cutoff k_{max} with $\Lambda = 500 \text{ MeV}$ for two values of the cubic box size, $L = 10 \text{ fm}$ (dashed line to guide the eye and open symbols) and $L = 13.4 \text{ fm}$ (solid line and filled symbols).

B. Results for a high regularization cutoff

First we use a regularization cutoff $\Lambda = 1000 \text{ MeV}$. Disregarding the spurious bound-state problem, we obtain a positive ground-state energy. Although the total energy is well converged, this solution is not physical as it corresponds to a discretized unbound solution. Correlatively the charge radius is very large. In fact it is found to oscillate between two distinct values larger than 5 fm . We checked that the same solution is reached when starting from an extremely deep and wide Woods–Saxon potential. This unbound solution results from a too strongly repulsive contact potential in the 3S_1 channel. Moreover removing the effect of the 3P_0 spurious bound state is expected to yield even more repulsion. Therefore in the rest of this subsection we do not further consider results with $\Lambda = 1000 \text{ MeV}$ and perform only calculations with $\Lambda = 1500 \text{ MeV}$.

Using $\Lambda = 1500 \text{ MeV}$ and disregarding first the spurious bound-state correction, we obtain the ground-state energy and charge radius plotted as functions of the UV cutoff k_{max} in the top panel of Fig. 5. With a “small” box of edge length $L = 10 \text{ fm}$, the ground-state energy and the charge radius are found to be very close to the corresponding values obtained with $L = 13.4 \text{ fm}$, which establishes IR convergence at least up to $k_{\text{max}} = 6 \text{ fm}^{-1}$, the maximum single-particle cutoff that our computation resources allow us to consider with the “large” box. Using the small box allows us to push further calculations, up to $k_{\text{max}} = 7 \text{ fm}^{-1}$. However this value of k_{max} is not enough to exhibit UV convergence. Finally we checked that,

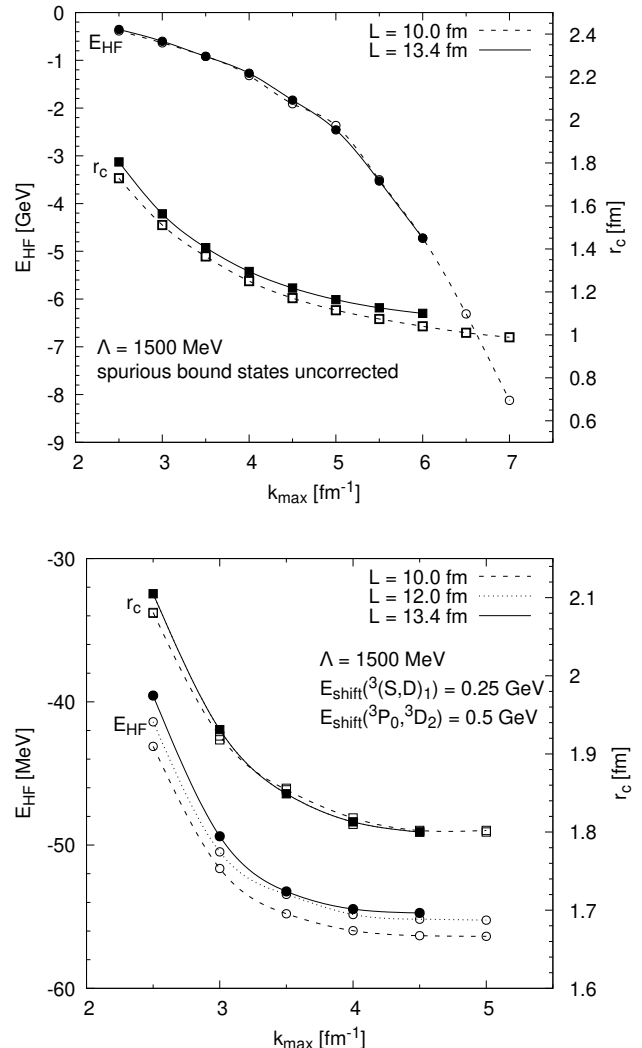


FIG. 5. Ground-state energy E_{HF} in the Hartree–Fock solution of ^{16}O as a function of the single-particle momentum cutoff k_{max} with $\Lambda = 1500 \text{ MeV}$ for various box sizes L without (top panel) and with (bottom panel) correction for spurious bound states. Symbols show calculated values, whereas the curves serve to guide the eye.

as for the low-regularization cutoff $\Lambda = 500 \text{ MeV}$, our Hartree–Fock ground-state solutions $|\Phi\rangle$ obtained with both box sizes $L = 10 \text{ fm}$ and $L = 13.4 \text{ fm}$, satisfy Eqs. (9a) to (9c). Moreover, with the smaller box of edge length $L = 10 \text{ fm}$, the values of $|\beta_4|$ are sizable, of the order of 0.1 to 0.2, while they are of the order of a few hundredths with the larger box of edge length $L = 13.4 \text{ fm}$. We attribute this difference to a smaller value of $\langle \Phi | r^4 | \Phi \rangle$ obtained with the smaller box, similarly to the slightly smaller charge-radius values for $L = 10 \text{ fm}$ than with $L = 13.4 \text{ fm}$ as can be seen on the top panel of Fig. 5. Therefore we can expect much smaller values of β_4 when correcting for spurious bound states, even partly, because the repulsion introduced by the corrective terms

should increase $\langle \Phi | r^4 | \Phi \rangle$ (as well as the charge radius).

Let us now address the correction of spurious bound states in the two-nucleon potential. The Hartree–Fock ground-state solution should not be bound if the energy shifts are too large, and it turns out that the recommended values of Ref. [12] are far above the maximal values yielding bound Hartree–Fock solutions. Moreover bound solutions obtained with spurious bound-states correction are expected to be very sensitive to the energy shifts. In this context our twofold goal is (i) to find a choice of simultaneous energy shifts for which IR and UV convergence are reached and (ii) to probe the response of the Hartree–Fock ground-state energy and charge radius to the energy shift in each channel supporting a spurious bound state.

Such a possible set of energy shifts is, for example, $E_{\text{shift}}(^3(S, D)_1) = 0.25$ GeV and $E_{\text{shift}}(^3P_0) = E_{\text{shift}}(^3D_2) = 0.5$ GeV, and yields the results shown in the bottom panel of Fig. 5 as functions of k_{max} for three different box sizes. As can be seen, the repulsion brought by the spurious bound-state correction provides UV convergence for $k_{\text{max}} \gtrsim 4$ fm⁻¹. Moreover IR convergence is again reached for edge lengths somewhat larger than $L = 10$ fm. It is therefore appropriate to use the single-particle basis parameters $k_{\text{max}} = 4$ fm⁻¹ and $L = 10$ fm to study the variation of the ground-state energy and the charge radius with the energy shift in each of the $^3(S, D)_1$, 3P_0 and 3D_2 channels, around the above set of E_{shift} values. The corresponding results are displayed in the left panels of Fig. 6, whereas the right panels show the partial-wave contributions to the nuclear interaction energy. Overall the sensitivity of E_{HF} and r_c to the energy shift is decreasing as the relative orbital-angular momentum increases. This is consistent with the fact that, in these observables, S -wave contributions to the NN potential dominate over the P -wave contributions, which themselves are larger than the D -waves. This hierarchy is observed in phenomenological effective “interactions” such as those of the Skyrme type, and seems to reflect the centrifugal suppression at work in two-nucleon phaseshifts. It is worth noting that, in the 3D_2 partial wave, it is even possible to apply energy shifts as large as 100 GeV without getting unbound solutions. Therefore, it is possible to completely correct for the spurious bound state in the 3D_2 channel using recommended values of Ref. [12]. However the Hartree–Fock ground-state solution does not converge as a function of $E_{\text{shift}}(^3D_2)$. Indeed if the strength E_{shift} of the corrected 3D_2 potential tends to $+\infty$, then its one-body reduction (the mean-field potential) becomes increasingly repulsive for any finite one-body density, so the single-particle states become unbound and the iterative process tend to diverge.

Another general observation from Fig. 6 is that, regardless of the channel in which the energy shift is applied, all partial-wave contributions to the nuclear interaction energy E_{int} decrease in absolute value and, with the exception of 3S_1 , even seem to converge with E_{shift} .

Therefore the non convergence of the Hartree–Fock solution with E_{shift} seems to be due to the 3S_1 channel of the NN potential. It is worth noting that despite its strong repulsive matrix elements, the 1S_0 NN potential gives a sizable negative contribution to E_{int} (hence attraction) as the energy shift increases beyond some value which depends on the spurious-bound-state channel. This is a highly nonlinear effect resulting from the Hartree–Fock procedure.

Finally it is worth mentioning that our partially corrected results in Fig. 5 all correspond to octahedral-symmetric solutions, obeying Eqs. (9a) to (9c), with very small β_4 values of the order of a few thousandths for all considered box sizes. Therefore the ground-state shapes are very close to spherical ones.

V. DISCUSSION

From the above results we conclude that the energy shift tends to suppress nuclear binding in the Hartree–Fock solution in addition to introducing a strong dependence on the energy shift. In fact we can even expect that no bound solution can be obtained at the Hartree–Fock level when using recommended values of energy-shift parameters $E_{\text{shift}}^{(i)}$ (10 to 15 GeV according to Ref. [12]).

This situation is at variance with the ab initio many-body methods based on the diagonalization of the nuclear Hamiltonian \hat{H} , such as the No-Core Shell Model. Up to truncation effects, solving the eigenvalue equation of $\hat{H}' = \hat{H} + \sum_i E_{\text{shift}}^{(i)} |\chi_i\rangle\langle\chi_i|$ yields low-energy solutions approximately independent of $E_{\text{shift}}^{(i)}$ (positive) values provided they are large enough. A residual dependence is expected because of the truncation of the underlying one-body harmonic-oscillator basis and the many-body basis. According to the Ritz variational principle, the energy functional is stationary around the eigenstates of \hat{H} if one works in the full Hilbert space. Therefore one expects that, if the trial wavefunction of the variational principle was rich enough, one would get a $E_{\text{shift}}^{(i)}$ -independent result for the ground state if $E_{\text{shift}}^{(i)}$ values are large enough to decouple the spurious bound states from the physical ones. The extreme sensitivity of the Hartree–Fock ground-state solution can thus be attributed to its Slater determinant form, in other words to its breaking of translation symmetry and the lack of beyond-mean-field correlations (in particular those associated with the restoration of broken symmetries). This clearly shows that not only the Hartree–Fock approximation, and related approaches like the Hartree–Fock–Bogoliubov approach (which variationally incorporates one-body effects of pairing correlations), intrinsically break renormalization-group invariance, but they cannot even provide a reference solution for beyond mean-field calculations if one tries to implement a full correction for spurious bound-state effects.

A possible way out in mean-field based approaches is

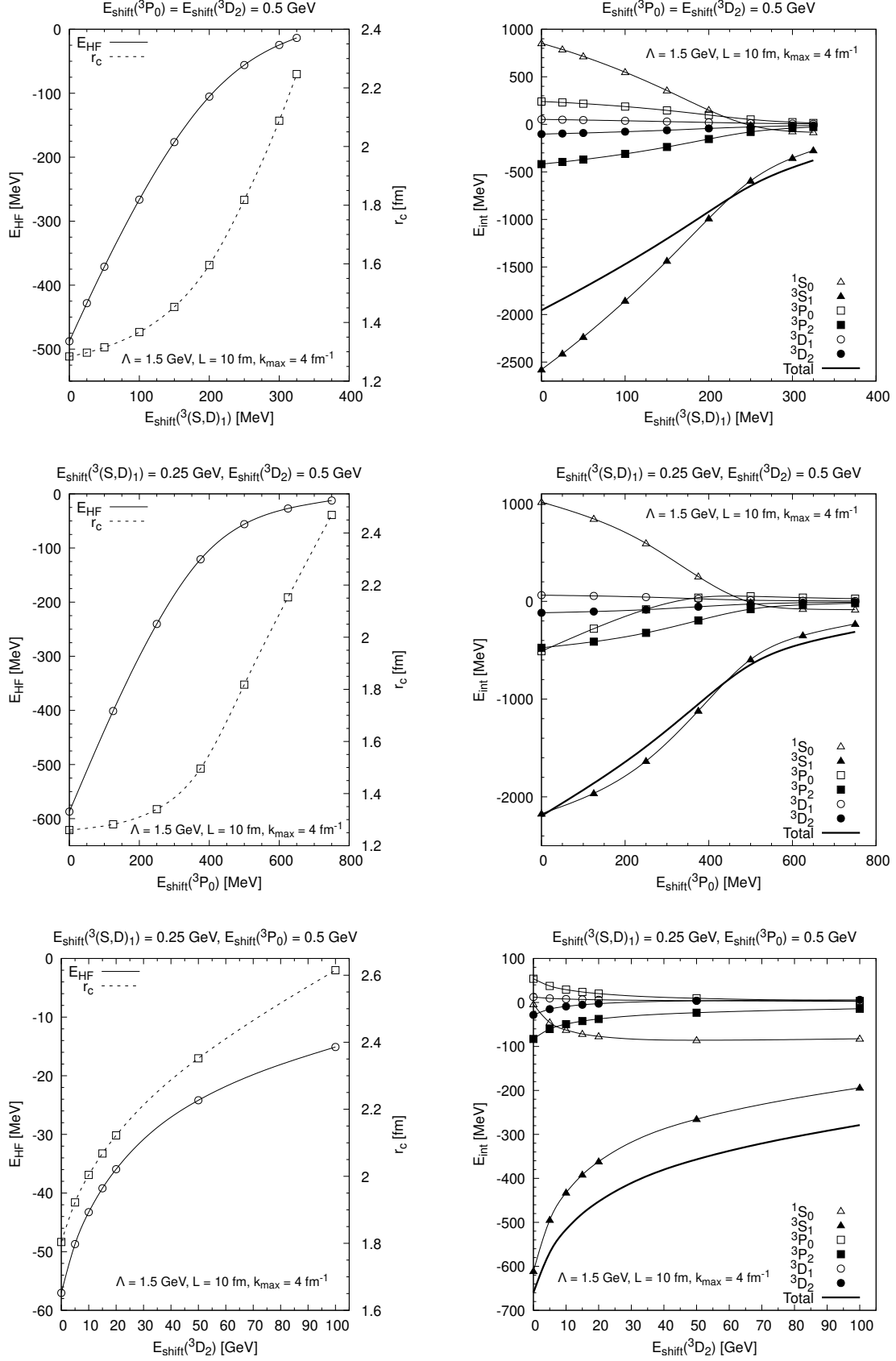


FIG. 6. Left panels: ground-state energy E_{HF} (open circles, left scale) and charge radius (squares, right scale) in the Hartree–Fock solution of ${}^{16}\text{O}$ as a function of the energy shift in the ${}^3(S,D)_1$ (top row), 3P_0 (middle row) and 3D_2 (bottom row) channels with a box size $L = 10$ fm and a single-particle momentum cutoff $k_{\text{max}} = 4$ fm $^{-1}$. Right panels: interaction energy $E_{\text{int}} = \langle \Phi | \hat{V}_{\text{NN}} | \Phi \rangle$ as a function of the energy shift in the corresponding channels.

to split the spurious-bound-state correction term into a contribution treated at the mean-field level and the remaining one treated together with the residual interaction beyond mean field. This allows to bring in enough repulsion to effectively “soften” the inter-nucleon potential and yield a UV convergence of mean-field results for tractable single-particle bases, without compromising the bound character of the ground-state solutions. We can even correct “fully” for the 3D_2 spurious bound states by employing energy shifts of the order of 15 to 20 GeV as recommended by Yang and collaborators [12]. Indeed such large values of E_{shift} , and even somewhat larger ones, do not prevent from obtaining bound Hartree–Fock solutions as shown in the last row of Fig. 6. However one has to keep in mind that, as shown by the results with the $\Lambda = 1$ GeV regularization cutoff, mean-field bound solutions can be obtained only for Λ values for which the contact potential is attractive. Because the 3S_1 channel is dominant, this corresponds essentially to $C_{3S_1}(\Lambda) < 0$.

VI. CONCLUSIONS

After renormalizing the one-pion-exchange potential in the Nogga–Timmermans–van Kolck power counting at leading order, we attempted Hartree–Fock calculations in ${}^{16}\text{O}$ with a regularization cutoff Λ up to 1500 MeV. The single-particle wave functions and the potential matrix elements are represented in a basis of plane waves confined in a cubic box of edge length several times larger than the nuclear radius and truncated according to the norm of the single-particle momentum. The largest relative momentum retained in the potential matrix elements thus identifies with this single-particle momentum cutoff.

In this framework we first highlighted the strong sensitivity of the Hartree–Fock ground-state solution to the regularization cutoff Λ as a direct consequence of the running of the low-energy constants in partial-wave channels where the one-pion-exchange potential is attractive and singular (exhibiting a limit-cycle-like behavior). In particular we identified the 3S_1 counter-term as being dominantly responsible for either an extremely attractive or a strongly repulsive renormalized potential. In addition to this behavior, the two-nucleon renormalized potential can yield spurious deeply bound states in the two-nucleon system, which requires a correction in order to remove the unphysical excess of attraction above some value of Λ . This is done by adding to the potential the projectors on the spurious bound states with a weight playing the role of an energy shift. We analyzed the effect on the Hartree–Fock ground-state solution of the corrected potential as a function of the energy shift and the partial-wave channel. We found a weak dependence on the 3D_2 energy shift, making so-corrected Hartree–Fock calculations meaningful. However, in stark contrast, even a modest energy shift in the 3S_1 or 3P_0 channels completely suppresses nuclear binding in the Hartree–Fock solution.

From this study we conclude that one cannot build

a Hartree–Fock solution free of spurious-bound-state effects that can serve as a reference state for many-body approaches such as coupled cluster or in-medium SRG. The treatment of the spurious bound states has thus to be implemented at least partly beyond Hartree–Fock. We showed that a partial treatment of the corrected two-nucleon potential at the Hartree–Fock level can be done with a single-particle basis with a momentum cutoff significantly below the regularization cutoff Λ of the potential. This makes feasible such partly corrected calculations even for high values of Λ . However the remaining part of the corrected two-nucleon potential has to be treated beyond the Hartree–Fock approximation and this requires high momentum truncations, which is extremely challenging (see, e.g., Ref. [13]).

ACKNOWLEDGMENTS

We thank U. van Kolck, M. Pavón Valderrama and C.-J. Yang for valuable discussions. Part of computer time for this study was provided by the computing facilities MCIA (Mésocentre de Calcul Intensif Aquitain) of the Université de Bordeaux and of the Université de Pau et des Pays de l’Adour.

Appendix A: One-pion exchange potential

In momentum space the one-pion exchange (nonrelativistic) potential takes the form

$$\langle \mathbf{k}' | \hat{V}_{1\pi}^{(0)} | \mathbf{k} \rangle = W_{T,1\pi}(q) (\hat{\sigma}_1 \cdot \mathbf{q})(\hat{\sigma}_2 \cdot \mathbf{q})(\hat{\tau}_1 \cdot \hat{\tau}_2) \quad (\text{A1a})$$

where \mathbf{k}, \mathbf{k}' are incoming and outgoing relative momenta, $\hat{\sigma}_i$ and $\hat{\tau}_i$ are Pauli spin and isospin operators, and the form factor $W_{T,1\pi}(q)$ reads

$$W_{T,1\pi}(q) = - \left(\frac{g_A}{2f_\pi} \right)^2 \frac{(\hbar c)^3}{q^2 + \Lambda_\pi^2}. \quad (\text{A1b})$$

This potential depends only on the momentum transfer $\mathbf{q} = \mathbf{k}' - \mathbf{k}$ owing to its local character. We introduce the notation $\Lambda_\pi = \frac{m_\pi c^2}{\hbar c}$ for the inverse of the reduced Compton wavelength of the pion. Here m_π represents the mean pion mass. In coordinate space the one-pion exchange potential is given by

$$\langle \mathbf{r}' | \hat{V}_{\text{LO}} | \mathbf{r} \rangle = \delta(\mathbf{r}' - \mathbf{r}) V_{1\pi}(\mathbf{r}) \quad (\text{A2a})$$

where

$$V_{1\pi}(\mathbf{r}) = \frac{(2\pi)^3}{N_k} \frac{(m_\pi c^2)^3}{12\pi} \left(\frac{g_A}{2f_\pi} \right)^2 (\hat{\tau}_1 \cdot \hat{\tau}_2) \left[T_{1\pi}(\Lambda_\pi r) \hat{S}_{12} + \left(Y_{1\pi}(\Lambda_\pi r) - \frac{4\pi}{\Lambda_\pi^3} \delta(\mathbf{r}) \right) \hat{\sigma}_1 \cdot \hat{\sigma}_2 \right], \quad (\text{A2b})$$

The constant N_k is a plane-wave normalization factor defined by

$$\langle \mathbf{k}' | \mathbf{k} \rangle = N_k \delta(\mathbf{k}' - \mathbf{k}), \quad (\text{A3a})$$

hence the following expression of the plane wave in coordinate space

$$\langle \mathbf{r} | \mathbf{k} \rangle = \sqrt{\frac{N_k}{(2\pi)^3}} e^{i\mathbf{k}\cdot\mathbf{r}}. \quad (\text{A3b})$$

The usual tensor operator \hat{S}_{12} reads

$$\hat{S}_{12} = \frac{3}{r^2} \{ \mathbf{r} \otimes \mathbf{r} \}_2 \cdot \{ \hat{\boldsymbol{\sigma}}_1 \otimes \hat{\boldsymbol{\sigma}}_2 \}_2 = 3(\hat{\boldsymbol{\sigma}}_1 \cdot \hat{r})(\hat{\boldsymbol{\sigma}}_2 \cdot \hat{r}) - \hat{\boldsymbol{\sigma}}_1 \cdot \hat{\boldsymbol{\sigma}}_2 \quad (\text{A4})$$

where $\hat{r} = \mathbf{r}/r$ is unit vector and $\{A \otimes B\}_k$ denotes the irreducible tensor product of rank k of spherical tensors A and B according to the notation and definition of Varshalovich et al. [49]. The functions $Y_{1\pi}$ and $T_{1\pi}$ are defined as

$$Y_{1\pi}(x) = \frac{e^{-x}}{x} \quad (\text{A5a})$$

$$T_{1\pi}(x) = Y_{1\pi}(x) \left(1 + \frac{3}{x} + \frac{3}{x^2} \right). \quad (\text{A5b})$$

Appendix B: Low-energy constants

a. 1S_0 channel. The three LECs Δ_1 , Δ_2 , γ in Eq. (6) are fitted to reproduce the effective-range expansion (scattering length $a_0 = -23.75$ fm and effective-range parameter $r_0 = 2.77$ fm as used in Ref. [10]) and the vanishing of the phase shift at $\hbar c k_0 \approx 350$ MeV as used in Ref. [38]. The values of physical constants retained in our adjustment of LECs are $\hbar c = 197.327$ MeV · fm, $2\mu c^2 = 938.918$ MeV, $g_A = 1.26$, $f_\pi = 92.4$ MeV and $m_\pi c^2 = 138.03$ MeV. Table II shows the resulting values for several values of the momentum cutoff Λ , whereas figure 7 shows the resulting phaseshift for $\Lambda = 1500$ MeV and illustrates in particular the successful fit of k_0 .

TABLE II. Low-energy constants Δ_1 , Δ_2 and γ (in MeV) for various values of Λ in Eq. (2).

Λ (MeV)	Δ_1 (MeV)	Δ_2 (MeV)	γ (MeV)
500	-89.4	473.0	312.0
1000	-81.2	282.8	274.4
1500	-94.3	319.1	243.1

For completeness we also give the partial-wave matrix elements of the one-pion exchange potential (including the regularization function) in 1S_0 and 3S_1 channels

$$\begin{aligned} V_{1\pi}^{(^1S_0)}(k', k) &= V_{1\pi}^{(^3S_1)}(k', k) \\ &= \frac{4\pi N'_k}{N_k} \left(\frac{g_A m_\pi c^2}{2f_\pi} \right)^2 \frac{\hbar c}{\Lambda_\pi^2} \left[1 - \frac{\Lambda_\pi^2}{4k'k} \times \right. \\ &\quad \left. \ln \left(\frac{(k' + k)^2 + \Lambda_\pi^2}{(k' - k)^2 + \Lambda_\pi^2} \right) \right] f_{\text{reg}}(k', k). \quad (\text{B1}) \end{aligned}$$

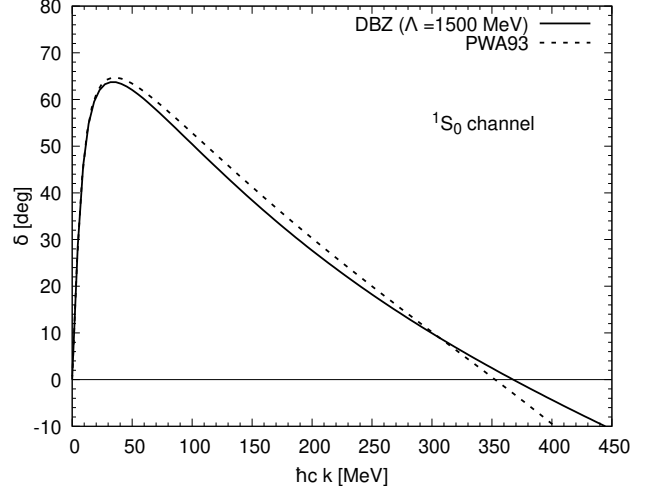


FIG. 7. Phaseshift in the 1S_0 channel with the DBZ counterterm and the LECs values of Table II for $\Lambda = 1500$ MeV (solid line), compared with the empirical one from the Nijmegen multi-energy np analysis [50] (PWA93, dashed line).

b. 3S_1 channel. In this work we choose to write regularized partial-wave matrix elements of \hat{V}_{ct} in the 3S_1 channel as

$$V_{\text{ct}}^{(^3S_1)}(k', k) = \frac{4\pi N'_k}{N_k} C_{3S_1} \frac{\hbar c}{\Lambda_\pi^2} \times f_{\text{reg}}(k', k). \quad (\text{B2})$$

The LEC C_{3S_1} is dimensionless and adjusted to the np scattering length ($a^{(^3S_1)} = 5.42$ fm as used in Ref. [8]) as a function of the regularization cutoff Λ by solving the Lippmann–Schwinger equation. The coupling to the D wave is taken into account.

For the same values of Λ as above, we find the LEC values reported in table III. We also provide the predicted effective-range parameter r_0 , reasonably independent of Λ and close to its value 1.75 fm deduced, e.g, from the Nijmegen partial-wave analysis [50]. As expected from

TABLE III. Values of the low-energy constant in the 3S_1 partial wave for various values of Λ in Eq. (2) fitted to the scattering length and predicted effective-range parameter r_0 .

Λ (MeV)	C_{3S_1}	$C_{3S_1} \frac{\hbar c}{\Lambda_\pi^2}$ (MeV · fm ³)	r_0 (fm)
500	-1.19815	-483.20	1.50
1000	+8.2743	+3336.90	1.65
1500	-2.36022	-951.84	1.63

the singular and attractive character of the tensor potential in the coupled partial waves, and as already observed by Nogga and collaborators [8], the LEC in the 3S_1 channel exhibits a limit-cycle-like behavior in its variation with Λ . In particular these authors, who use the regularization function of Eq. (2), find a vertical asymptote for $\Lambda \approx 1250$ MeV. This explains the large positive

TABLE IV. Low-energy constants in the 3P_0 , 3P_2 and 3D_2 channels for several values of Λ in Eq. (2).

Λ (MeV)	$C_{3P_0}(\times 10^{-4})$	$C_{3P_0} \frac{\hbar c}{\Lambda^4}$ (MeV · fm ⁵)	$C_{3P_2}(\times 10^{-4})$	$C_{3P_2} \frac{\hbar c}{\Lambda^4}$ (MeV · fm ⁵)	$C_{3D_2}(\times 10^{-4})$	$C_{3D_2} \frac{\hbar c}{\Lambda^6}$ (MeV · fm ⁷)
500	2315.915	190.88	-732.28	-60.36	-31.643	-5.33
1000	-522.851	-43.09	-244.57	-20.16	+8.353	1.41
1500	-3.189	-0.26	-88.942	-7.33	-3.214	-0.54

value of C_{3S_1} for $\Lambda = 1000$ MeV and its large negative value for $\Lambda = 1500$ MeV.

c. 3P_0 , 3P_2 and 3D_2 channels. The counter terms in these channels are written in the form

$$V_{\text{ct}}^{(3P_0)}(k', k) = 4\pi \frac{N'_k}{N_k} C_{3P_0} \frac{\hbar c}{\Lambda_\pi^2} \frac{k'k}{\Lambda_\pi^2} \quad (\text{B3})$$

$$V_{\text{ct}}^{(3P_2)}(k', k) = 4\pi \frac{N'_k}{N_k} C_{3P_2} \frac{\hbar c}{\Lambda_\pi^2} \frac{k'k}{\Lambda_\pi^2} \quad (\text{B4})$$

$$V_{\text{ct}}^{(3D_2)}(k', k) = 4\pi \frac{N'_k}{N_k} C_{3D_2} \frac{\hbar c}{\Lambda_\pi^2} \frac{(k'k)^2}{\Lambda_\pi^4}. \quad (\text{B5})$$

The dimensionless low-energy constants C_{3P_0} and C_{3P_2} have been adjusted to the phase shifts at $T_{lab}(k) = 2(\hbar k)^2/(2\mu) = 50$ MeV from the Nijmegen partial-wave analysis [50], namely $\delta^{(3P_0)} = 10.7^\circ$ and $\delta^{(3P_2)} = 5.9^\circ$, whereas C_{3D_2} has been adjusted to the phase shift at $T_{lab}(k) = 2(\hbar k)^2/(2\mu) = 100$ MeV, namely $\delta^{(3D_2)}(k) = 17.3^\circ$. The results of the fits are displayed in Table IV.

Appendix C: Confined plane-wave basis

1. Basis wave functions confined in a box

In coordinate space these confined plane waves take the form

$$\langle \mathbf{r} | \varphi_\alpha \rangle = \varphi_\alpha(\mathbf{r}) = \begin{cases} L^{-3/2} e^{i\mathbf{k}_\alpha \cdot \mathbf{r}} & \text{if } \mathbf{r} \in \left[-\frac{L}{2}; \frac{L}{2}\right]^3 \\ 0 & \text{otherwise.} \end{cases} \quad (\text{C1})$$

where L is the edge length and α is a triplet of indices $(\alpha_x, \alpha_y, \alpha_z)$ specified by the orthogonality condition

$$\langle \varphi_{\alpha'} | \varphi_\alpha \rangle = \delta_{\alpha'\alpha} = \delta_{\alpha'_x \alpha_x} \delta_{\alpha'_y \alpha_y} \delta_{\alpha'_z \alpha_z}. \quad (\text{C2})$$

This condition is satisfied in particular for momentum vectors $\mathbf{k}_\alpha = (k_{\alpha_x}, k_{\alpha_y}, k_{\alpha_z})$ (in the cartesian basis) such that $k_{\alpha_x} = \alpha_x \frac{2\pi}{L}$ with either $\alpha_x \in \mathbb{Z}$ or $\alpha_x - \frac{1}{2} \in \mathbb{Z}$, and similarly for the other space directions. Here we choose the latter case to obtain non vanishing momentum values. We thus denote by $|\varphi_{\alpha\sigma\tau}\rangle$ the basis states, which are infinite in number up to this point.

It turns out that, in one dimension (for example the x direction), the wave function

$$\varphi_{\alpha_x}(x) = \begin{cases} L^{-1/2} e^{ik_{\alpha_x} x} & \text{if } x \in \left[-\frac{L}{2}; \frac{L}{2}\right] \\ 0 & \text{otherwise,} \end{cases} \quad (\text{C3})$$

is the variational basis of the Lagrange-mesh method associated with an equidistant mesh on the x axis over the interval $[-\frac{L}{2}; +\frac{L}{2}]$ [40]. This finite mesh, called the Lagrange-Fourier mesh, is made of the N abscissa $x_m = m dx$ with the mesh step $dx = \frac{L}{N}$ and $m \in I_N$ where

$$I_N = \left\{ -\frac{N-1}{2}, -\frac{N-1}{2} + 1, \dots, \frac{N-1}{2} \right\}. \quad (\text{C4})$$

The Lagrange functions $f_j(x)$, with $j \in I_N$, associated with this mesh are such that $f_j(x_m) = \delta_{jm}$ and are orthogonal to each other at the Gauss-quadrature approximation based on this mesh. The two sets of functions $\{f_j(x), j \in I_N\}$ and $\{\varphi_{\alpha_x}(x), \alpha_x \in I_N\}$ are related by a unitary transformation (see section 2.2 of Ref. [40]). This offers a dual interpretation of the confined plane-wave basis and its parameters L and N (or equivalently L and dx such that $L/dx \in \mathbb{N}^*$). In all rigor the set of orthonormal states $\{|\varphi_{\alpha_x}\rangle, \alpha_x \in I_N\}$ is a Hilbert basis of the Hilbert space of square integrable functions over the interval $[-\frac{L}{2}; +\frac{L}{2}]$ only in the limit $N \rightarrow \infty$.

Because $(I_N, \mathbb{N}^*, \subset)$ is an increasing sequence for inclusion, the parameter N (or dx) for a fixed edge length L is a variational parameter for Hartree-Fock calculations. Indeed increasing N brings additional states in the single-particle basis and thus always yield ground-state solutions lower in energy. In contrast increasing L does not necessarily produce lower-energy solutions, but approximate solutions expectedly closer to the exact ones which correspond to an infinite box size.

2. Symmetry-adapted basis

The set of $|\varphi_{\alpha\sigma}\rangle$ for a fixed isospin projection, corresponding to either neutron or proton single-particle states, is a basis of reducible co-representation of the full octahedral double group with time-reversal symmetry, denoted by O_{2h}^{DT} . We build a symmetry-adapted basis by a subsequent unitary transformation so that the resulting orthonormal set of states is a basis of reducible co-representation of a subgroup G of O_{2h}^{DT} . We choose here the subgroup $G = \text{Gr}\{\hat{\Pi}, \hat{R}_z, \hat{R}_y^T\}$ generated by the parity operator $\hat{\Pi}$, the z -signature operator \hat{R}_z and the antiunitary operator $\hat{R}_y^T = \hat{T}\hat{R}_y$ where \hat{T} is the time-reversal operator. Even if we consider, in this work, time-reversal invariant solutions only, it is more advantageous not to add \hat{T} to the above symmetry group G , which would yield

the full dihedral double group with time-reversal symmetry D_{2h}^{DT} . Indeed the unitary subgroup $\text{Gr}\{\hat{\Pi}, \hat{R}_z\}$ of G is abelian and yields two quantum numbers (intrinsic parity and z -signature), whereas the unitary subgroup $\text{Gr}\{\hat{\Pi}, \hat{R}_z, \hat{R}_y\}$ of D_{2h}^{DT} is non abelian and yields only one quantum number (intrinsic parity). Moreover in both cases one can reduce the set of discretized momenta to one eighth of the full three-dimensional mesh in order to generate a basis of corepresentation of O_{2h}^{DT} .

The symmetry-adapted basis in the present case is obtained by a proper unitary transformation of the above defined confined plane-wave basis. It can be constructed by use of projection operators

$$\hat{P}(p) = \frac{1}{2} \left(\mathbb{1} + \frac{\hat{\Pi}}{p} \right) \quad (\text{C5a})$$

$$\hat{P}(r_z) = \frac{1}{2} \left(\mathbb{1} + \frac{\hat{R}_z}{r_z} \right) \quad (\text{C5b})$$

where $p = \pm 1$ and $r_z = \pm i$ are the intrinsic-parity and

z -signature quantum numbers. Moreover, defining the operator $\hat{Q}_c = \frac{1}{2}(\mathbb{1} + c\hat{R}_y^T)$, with $c = \pm 1$, one can show that for fixed (p, r_z) , $\alpha = (\alpha_x, \alpha_y, \alpha_z)$, with $\alpha_m - \frac{1}{2} \in \mathbb{N}$ ($m = x, y, z$) and $\sigma = \pm \frac{1}{2}$, the two states

$$|pr_z(c\alpha\sigma)\rangle = \sqrt{8} \hat{P}(p) \hat{P}(r_z) \hat{Q}_c |\varphi_{\alpha\sigma}\rangle, \quad c = \pm 1, \quad (\text{C6})$$

form two bases of equivalent irreducible corepresentations of G of dimension 1. Note that here we have chosen to work with α being a half-integer triplet, that is even N values, therefore all α_m indices are different from 0.

3. Linear-momentum property of the confined plane-wave basis

We first write the matrix element of a two-body potential \hat{V} between confined plane-wave states through the coordinate representation of these states as

$$\langle \varphi_{\alpha'_1} \varphi_{\alpha'_2} | \hat{V} | \varphi_{\alpha_1} \varphi_{\alpha_2} \rangle = L^{-6} \int_{\mathcal{C}_{L/2}} d^3 \mathbf{r}'_1 \int_{\mathcal{C}_{L/2}} d^3 \mathbf{r}'_2 \int_{\mathcal{C}_{L/2}} d^3 \mathbf{r}_1 \int_{\mathcal{C}_{L/2}} d^3 \mathbf{r}_2 e^{i(\mathbf{k}_{\alpha_1} \cdot \mathbf{r}_1 + \mathbf{k}_{\alpha_2} \cdot \mathbf{r}_2 - \mathbf{k}_{\alpha'_1} \cdot \mathbf{r}'_1 - \mathbf{k}_{\alpha'_2} \cdot \mathbf{r}'_2)} \langle \mathbf{r}'_1 \mathbf{r}'_2 | \hat{V} | \mathbf{r}_1 \mathbf{r}_2 \rangle, \quad (\text{C7})$$

where $\mathcal{C}_{L/2} = [-\frac{L}{2}; +\frac{L}{2}]^3$. Owing to Galilean and translation invariances of \hat{V} , the matrix element $\langle \mathbf{r}'_1 \mathbf{r}'_2 | \hat{V} | \mathbf{r}_1 \mathbf{r}_2 \rangle$ is of the form

$$\langle \mathbf{r}'_1 \mathbf{r}'_2 | \hat{V} | \mathbf{r}_1 \mathbf{r}_2 \rangle = \delta(\mathbf{R}' - \mathbf{R}) \langle \mathbf{r}' | \hat{V} | \mathbf{r} \rangle \quad (\text{C8})$$

where $\mathbf{R} = \frac{1}{2}(\mathbf{r}_1 + \mathbf{r}_2)$ is the center-of-mass position vector and $\mathbf{r} = \mathbf{r}_1 - \mathbf{r}_2$ (similarly for \mathbf{r}') is the relative position vector. Using these substitutions in the integrals of Eq. (C7) we obtain

$$\langle \varphi_{\alpha'_1} \varphi_{\alpha'_2} | \hat{V} | \varphi_{\alpha_1} \varphi_{\alpha_2} \rangle = L^{-6} \int_{\mathcal{C}_L} d^3 \mathbf{r}' \int_{\mathcal{C}_L} d^3 \mathbf{r} e^{i(\mathbf{k}_{\alpha'} \cdot \mathbf{r} - \mathbf{k}_{\alpha'} \cdot \mathbf{r}')} \times \langle \mathbf{r}' | \hat{V} | \mathbf{r} \rangle \int_{\mathcal{D}' \cap \mathcal{D}} d^3 \mathbf{R} e^{i(\mathbf{K}_{\alpha'} - \mathbf{K}_{\alpha}) \cdot \mathbf{R}} \quad (\text{C9})$$

where the domains of integration \mathcal{C}_L , \mathcal{D} and \mathcal{D}' are defined by

$$\mathcal{C}_L = \left[-\frac{L}{2}; +\frac{L}{2} \right]^3 \quad (\text{C10a})$$

$$\mathcal{D} = \mathcal{D}_x \times \mathcal{D}_y \times \mathcal{D}_z \quad (\text{C10b})$$

$$\mathcal{D}' = \mathcal{D}_{x'} \times \mathcal{D}_{y'} \times \mathcal{D}_{z'} \quad (\text{C10c})$$

with, for instance,

$$\mathcal{D}_x = \left[-\frac{L}{2} + \frac{|x|}{2}; \frac{L}{2} - \frac{|x|}{2} \right]. \quad (\text{C11})$$

Moreover in Eq. (C9) we have introduced the incoming relative momentum \mathbf{k}_{α} and incoming total momentum \mathbf{K}_{α} defined by

$$\mathbf{k}_{\alpha} = \frac{1}{2}(\mathbf{k}_{\alpha_1} - \mathbf{k}_{\alpha_2}) \quad (\text{C12})$$

$$\mathbf{K}_{\alpha} = \mathbf{k}_{\alpha_1} + \mathbf{k}_{\alpha_2}, \quad (\text{C13})$$

and similarly for outgoing momenta. Owing to the short range of the two-nucleon strong interaction \hat{V} , we can approximate the domains \mathcal{D} and \mathcal{D}' with \mathbb{R}^3 when the box size L is much larger than the range of \hat{V} . In this approximation the domain of integration over \mathbf{R} then becomes \mathbb{R}^3 and the integrals over \mathbf{R} on the one hand, and over \mathbf{r}' , \mathbf{r} on the other hand, can be factorized. We end up with

$$\langle \varphi_{\alpha'_1} \varphi_{\alpha'_2} | \hat{V} | \varphi_{\alpha_1} \varphi_{\alpha_2} \rangle \approx \delta_{\alpha'_1 + \alpha'_2, \alpha_1 + \alpha_2} \frac{1}{N_k} \left(\frac{2\pi}{L} \right)^3 \times \langle \mathbf{k}_{\alpha'} | \hat{V} | \mathbf{k}_{\alpha} \rangle, \quad (\text{C14})$$

where $\alpha_1 + \alpha_2$ is the triplet of integers $(\alpha_{1x} + \alpha_{2x}, \alpha_{1y} + \alpha_{2y}, \alpha_{1z} + \alpha_{2z})$, and the relative-momentum multi-index α reads

$$\alpha = \frac{1}{2}(\alpha_1 - \alpha_2) = \left(\frac{\alpha_{1x} - \alpha_{2x}}{2}, \frac{\alpha_{1y} - \alpha_{2y}}{2}, \frac{\alpha_{1z} - \alpha_{2z}}{2} \right).$$

Therefore in the confined plane-wave basis, the two-body matrix elements are simply proportional to the momen-

tum representation of the interaction. This is in contrast with other bases, such as the momentum partial-wave or harmonic-oscillator basis, where it is necessary to perform a transformation from the laboratory frame to the center-of-mass frame using vector brackets [51] or Moshinsky coefficients [52], respectively.

In addition to a simplified calculation, the confined plane-wave basis offers an economical representation of the two-body matrix elements of \hat{V} . Indeed the set

of distinct relative momenta in one dimension $k_{\alpha_x} = \frac{1}{2}(k_{\alpha_{1x}} - k_{\alpha_{2x}})$ generated by a set of equidistant single-particle momenta $k_{\alpha_{1x}}$ and $k_{\alpha_{2x}}$ (see subsection II.A) is $\{\frac{\pi}{L}\alpha_x, -N+1 \leq \alpha_x \leq N-1\}$ (by unit step), the cardinal of which is $2N-1$ instead of N^2 for a non-equidistant momentum set. This entails a considerable gain of memory to store the (antisymmetrized) two-body matrix elements of \hat{V} in the confined plane-wave basis.

-
- [1] S. Weinberg, *Phys. Lett. B* **251**, 288 (1990).
- [2] S. Weinberg, *Nucl. Phys. B* **363**, 3 (1991).
- [3] R. Machleidt and D. R. Entem, *Phys. Rep.* **503**, 1 (2011).
- [4] P. Gysbers, G. Hagen, J. D. Holt, G. R. Jansen, T. D. Morris, P. Navrátil, T. Papenbrock, S. Quaglioni, A. Schwenk, S. R. Stroberg, and K. A. Wendt, *Nature Physics* **15**, 428 (2019).
- [5] V. Somà, P. Navrátil, F. Raimondi, C. Barbieri, and T. Duguet, *Phys. Rev. C* **102**, 014318 (2020).
- [6] H. Hergert, *Front. Phys.* **8**, 379 (2020).
- [7] P. Maris, E. Epelbaum, R. J. Furnstahl, J. Golak, K. Hebeler, T. Hüther, H. Kamada, H. Krebs, U.-G. Meißner, J. A. Melendez, A. Nogga, P. Reinert, R. Roth, R. Skibiński, V. Soloviov, K. Topolnicki, J. P. Vary, Y. Volkotrub, H. Witała, and T. Wolfgruber, *arXiv:2012.12396v2* (2020).
- [8] A. Nogga, R. G. E. Timmermans, and U. van Kolck, *Phys. Rev. C* **72**, 054006 (2005).
- [9] R. Machleidt, P. Liu, D. R. Entem, and E. R. Arriola, *Phys. Rev. C* **81**, 024001 (2010).
- [10] Y.-H. Song, R. Lazauskas, and U. van Kolck, *Phys. Rev. C* **96**, 024002 (2017).
- [11] Y.-H. Song, R. Lazauskas, and U. van Kolck, *Phys. Rev. C* **100**, 019901(E) (2019).
- [12] C.-J. Yang, A. Ekström, C. Forssén, and G. Hagen, *Phys. Rev. C* **103**, 054304 (2021).
- [13] C.-J. Yang, A. Ekström, C. Forssén, G. H. G. Rupak, and U. van Kolck, 2109.13303v1 (2021).
- [14] E. Epelbaum and U.-G. Meißner, *arXiv:0609037v2* (2013).
- [15] B. Long, *Eur. Phys. J. E* **25**, 1641006 (2016).
- [16] E. Epelbaum, A. M. Gasparyan, J. Gegelia, and U.-G. Meißner, *Eur. Phys. J. A* **54**, 186 (2018).
- [17] M. P. Valderrama, *Eur. Phys. J. A* **55**, 55 (2019).
- [18] E. Epelbaum, A. M. Gasparyan, J. Gegelia, and U.-G. Meißner, *Eur. Phys. J. A* **55**, 56 (2019).
- [19] U. van Kolck, *Front. Phys.* **8**, 79 (2020).
- [20] J. C. Slater, *Phys. Rev.* **81**, 385 (1951).
- [21] J. Le Bloas, M. H. Koh, P. Quentin, L. Bonneau, and J. I. A. Ithnin, *Phys. Rev. C* **84**, 014310 (2011).
- [22] W. Glöckle, *The Quantum Mechanical Few-Body Problem* (Springer-Verlag, 1983).
- [23] G. Hagen, T. Papenbrock, M. Hjorth-Jensen, and D. J. Dean, *Rep. Prog. Phys.* **106**, 096302 (2014).
- [24] Z. H. Sun, C. A. Bell, G. Hagen, and T. Papenbrock, *Phys. Rev. C* **106**, L061302 (2014).
- [25] V. Somà, T. Duguet, and C. Barbieri, *Phys. Rev. C* **84**, 064317 (2011).
- [26] V. Somà, C. Barbieri, T. Duguet, and P. Navrátil, *Eur. Phys. J. A* **57**, 135 (2021).
- [27] B. Bally and M. Bender, *Phys. Rev. C* **103**, 024315 (2021).
- [28] A. Tichai, P. Arthuis, T. Duguet, H. Hergert, and V. Somà, *Phys. Lett. B* **786**, 195 (2018).
- [29] M. Frosini, T. Duguet, J.-P. Ebran, and V. Somà, *Eur. Phys. J. A* **58**, 62 (2022).
- [30] M. Frosini, T. Duguet, J.-P. Ebran, B. Bally, T. Mongelli, T.R.Rodriguez, R.Roth, and V. Somà, *Eur. Phys. J. A* **58**, 63 (2022).
- [31] M. Frosini, T. Duguet, J.-P. Ebran, B. Bally, H. Hergert, T. Rodriguez, R. Roth, J. M. Yao, and V. Somà, *Eur. Phys. J. A* **58**, 64 (2022).
- [32] K. Tsukiyama, S. K. Bogner, and A. Schwenk, *Phys. Rev. Lett.* **106**, 222502 (2011).
- [33] H. Hergert, S. K. Bogner, T. D. Morris, A. Schwenk, and K. Tsukiyama, *Phys. Rep.* **621**, 165 (2016).
- [34] S. Stroberg, A. Calci, H. Hergert, J. Holt, S. Bogner, R. Roth, and A. Schwenk, *Phys. Rev. Lett.* **118**, 032502 (2017).
- [35] M. P. Valderrama, M. Sánchez Sánchez, C.-J. Yang, B. Long, J. Carbonell, and U. van Kolck, *Phys. Rev. C* **95**, 054001 (2017).
- [36] M. Birse, *Phys. Rev. C* **74**, 014003 (2006).
- [37] S. Wu and B. Long, *Phys. Rev. C* **99**, 024003 (2019).
- [38] M. Sánchez Sánchez, N. A. Smirnova, A. M. Shirokov, P. Maris, and J. P. Vary, *Phys. Rev. C* **102**, 024324 (2020).
- [39] M. Sánchez Sánchez, C.-J. Yang, B. Long, and U. van Kolck, *Phys. Rev. C* **97**, 024001 (2018).
- [40] D. Baye, *Phys. Rep.* **565**, 1 (2015).
- [41] D. Hüber, H. Witała, A. Nogga, W. Glöckle, and H. Kamada, *Few-Body Systems* **22**, 107 (1997).
- [42] K. A. Wendt, R. J. Furnstahl, and R. J. Perry, *Phys. Rev. C* **83**, 034005 (2011).
- [43] E. N. E. van Dalen and H. Mütter, *Phys. Rev. C* **90**, 034312 (2014).
- [44] Dao Duy Duc, PhD thesis, University of Bordeaux <https://theses.hal.science/tel-02887649> (2019).
- [45] Dao Duy Duc and L. Bonneau, *Acta Phys. Pol. B Suppl.* **13**, 405 (2020).
- [46] J. Dudek, J. Dobaczewski, N. Dubray, A. Góźdz, V. Pangon, and N. Schunck, *Eur. Phys. J. A* **58**, 64 (2022).
- [47] J. Dudek, A. Góźdz, K. Mazurek, and H. Molique, *J. Phys. G: Nucl. Part. Phys.* **37**, 064032 (2010).
- [48] P. Ring and P. Schuck, *The nuclear many-body problem* (Springer-Verlag, 1980).
- [49] D. A. Varshalovich, A. N. Moskalev, and V. K. Kharkon-skii, *Quantum Theory of Angular Momentum* (World Scientific, Singapore, 1988).
- [50] V. G. J. Stoks, R. A. M. Klomp, M. C. M. Rentmeester,

- and J. J. de Swart, Phys. Rev. C **48**, 792 (1993).
- [51] C. W. Wong and D. M. Clement, Nucl. Phys. A **183**, 210 (1972).
- [52] M. Moshinsky, Nucl. Phys. **13**, 104 (1959).